UNIVERSITY OF CALIFORNIA,
IRVINE

Experimental Thermal Resistance Measurement of Thermal Diodes based on PEM Fuel Cell Structure

THESIS

submitted in partial satisfaction of the requirements
for the degree of

MASTER OF SCIENCE

in Mechanical Engineering

by

Yiheng Pang

Dissertation Committee:
Professor Yun Wang, Chair
Associate Professor Iryna Zenyuk
Assistant Professor Penghui Cao

2020

Table of Contents

LIST OF FIGURES

LIST OF TABLES

ACHNOWLEDGMENTS

I would like to express my deep sense of gratefulness to my committee chair, Professor Yun Wang, who has the enthusiasm and erudition in this field. He has been supportive and has given me the freedom to pursue various projects without objection. He also perseveres in exploring the beauty of natural science and conveying a spirit of adventure in regard to research and scholarship, and inspiring students to find their potentials. Professor Wang was and remains my best role model for a scientist, mentor, and teacher.

I would like to thank my thesis committee members, Professor Penghui Cao and Professor Iryna Zenyuk, for all of their guidance through this process; your discussion, ideas, and feedback have been absolutely invaluable. Their work inspired my thinking for thermal analysis and thermal conductivity measurements.

ABSTRACT OF THE DISSERTATION

Experimental Thermal Resistance Measurement of Thermal Diodes based on PEM Fuel Cell Structure

By

Yiheng Pang

Renewable Energy Resources Lab (RERL)

Department of Mechanical and Aerospace Engineering,

University of California, Irvine

Professor Yun Wang, Chair

This study reports experimental measurements of the thermal resistances of a thermal diode structure, consisting of microscale-thickness layers of distinct physical properties. The concept was developed based on the cathode structure of PEM fuel cell, which promotes water and heat removal in one direction by heat pipe effects in porous media. The diode layers have an overall thickness of 100-1,000 micrometers, similar to the overall thickness of the cathode in a PEM fuel cell. The unique thermal property is enabled by the heat pipe effects, directed by the arrangement of the sublayers through the capillary action. Experimental measurement is carried out on the simplest structure that consists of two sublayers with one being hydrophilic and the other hydrophobic. Various materials of distinct wettability properties are used and tested, including printing paper, carbon paper, cellulose paper, and polypropylene paper. The testing was also conducted under various conditions such as temperature,

water contents, and sublayer properties, which may greatly influence the unique thermal property of this type of thermal diodes. Two water contents, 40% and 60% (volume percent) and temperature range of 30 ˚C-90 ˚C were examined. Results show that under 90 ˚C and 60% water contents. we achieve resistance 0.280 K/W in the conductive direction, over three times smaller than that in the opposite direction (0.874 K/W) for cellulose paper and polypropylene paper materials. For the sample of printing paper with carbon paper, and the sample of cellulose paper with carbon paper, the thermal resistances also have about two times difference. The thermal diodicity increases with temperature and water content in the most cases. Future work is to fabricate the diodicity materials for larger than 10 thermal diodicity.

CHAPTER 1 INTRODUCTION

1.1 OVERVIEW OF HEAT TRANSFER

Heat transfer is a vital and enabling discipline across a range of emerging technologies including but not limited to information technology, biotechnology, pharmacology, and alternative energy generation. Heat transfer is thermal energy in transit due to spatial temperature difference [1]. When there exists a temperature difference in a medium or between media, heat transfer will occur. Figure 1 shows three types of heat transfer modes: conduction, convection, and radiation.

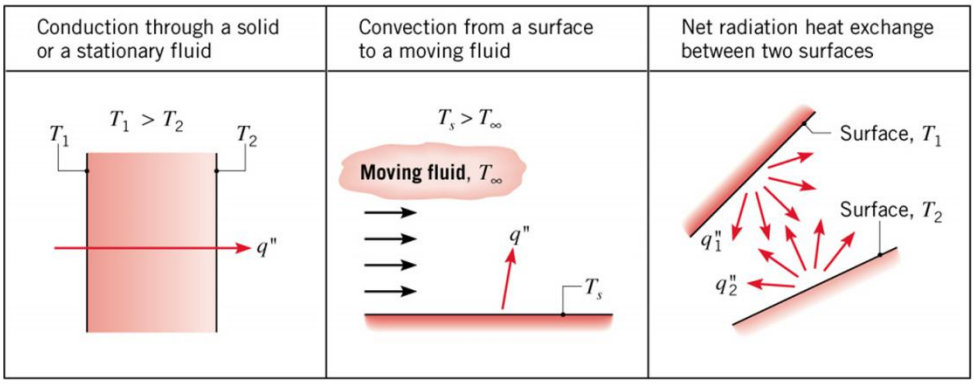

Figure 1. Conduction, convection, and radiation heat transfer modes [2]

Conduction may be viewed as the transfer of energy from the more energetic to the less energetic particles of a substance due to interactions between particles or molecules. Energy transfer by conduction must then occur in the direction of decreasing temperature. The convection heat transfer mode is promoted by bulk flows, or macroscopic motion of a fluid. Thermal radiation is energy emitted by matter that is at a nonzero temperature [1], transported by electromagnetic waves. While the

transfer of energy by conduction or convection requires the presence of a material medium, radiation does not.

1.2 PEM FUEL CELL

Polymer electrolyte membrane (PEM) fuel cells, which convert the chemical energy stored in hydrogen fuel directly and efficiently to electrical energy with water as the only byproduct, have the potential to reduce our energy use, pollutant emissions, and dependence on fossil fuels [3]. Figure 2 shows the basic process of PEM fuel cells. Hydrogen fuel is channeled through field flow plates to the anode on one side of the fuel cell, while oxygen from the air is channeled to the cathode on the other side of the cell. At the anode, a platinum catalyst causes the hydrogen to split into positive hydrogen ions (protons) and negatively charged electrons. The Polymer Electrolyte Membrane (PEM) allows only the positively charged ions to pass through it to the cathode. The negatively charged electrons must travel along an external circuit to the cathode, creating an electrical current. At the cathode, the electrons and positively charged hydrogen ions combine with oxygen to form water, which flows out of the cell [4-8]. The following electrochemical reactions occur on the active reaction surface:

Hydrogen oxide reaction: $H_2 \rightarrow 2H^+ + 2e^-$ (Anode)

Oxygen reduction reaction: $O_2 + 4e^- + 4H^+ \rightarrow 2H_2O$ (Cathode)

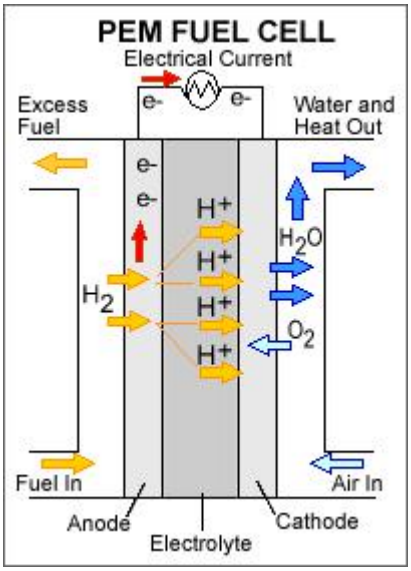

Figure 2. Schematic of PEM fuel cell [9]

In the past years, significant progress has been made in PEM fuel cell commercialization. By 2019, there were over 19,000 fuel cell electric vehicles (FCEV) and 340 hydrogen refueling stations (HRF) in the U.S. (~8,000 and 44, respectively), Japan (~3,600 and 112, respectively), South Korea (~5,000 and 34, respectively), Europe (~2,500 and 140, respectively), and China (~110 and 12, respectively). Japan, South Korea, and China plan to build approximately 3,000 HRF stations by 2030. In 2019, Hyundai Nexo and Toyota Mirai accounted for approximately 63% and 32% of the total sales, with a driving range of 380 and 312 miles and a mile per gallon (MPGe) of 65 and 67, respectively [10].

1.3 WATER AND THERMAL MANAGEMENT

Water management is a central issue in PEM fuel cell technology. The goal of water management is to balance two conflicting effects. One effect is to hydrate the

electrolyte. The ionic conductivity of the electrolyte depends on the membrane hydration level, and dryness increases membrane ionic resistance [4-5]. The other effect is to avoid excessive liquid water in fuel cells, which increases mass transport limitation. For PEM fuel cells, high water content increases the proton conductivity of membranes, reducing the ohmic voltage loss. Since liquid water formation is determined by the water vapor saturation pressure, the temperature field and its coupling with water condensation and evaporation are critical to the study of two-phase transport and the ensuing cathode excessive liquid water in a PEM fuel cell [11-12].

Thermal management is also crucial to PEM fuel cells, in which waste heat needs to be removed. The high variation of temperature, from inlet to outlet and from land to channel and from channel to land, is evident [13-14]. Some critical aspects of water and thermal management include [15-23]:

- Liquid water can dissolve materials such as sealing materials leading to contamination of membranes and catalyst layer.
- Excess water floods electrodes, hindering reactant transport to reaction sites and consequently leading to reactant starvation and material degradation.
- Dry operation subjects the electrolyte membrane to cracking or pinhole formation.
- Hot spot formation causes localized dryout and consequently membrane pinhole formation.
- Thermal cycles degrade fuel cell materials.

- Freezing cycles reduce the total area of active or catalytic surfaces, and hence electrode performance and durability.

To implement proper water and thermal management, water and heat generation in the cathode need to be adequately removed from the electrode to the channel. The fuel cell materials, such as channels, gas diffusion layer (GDL), and microporous layer (MPL), are also optimized in design in material properties including porosity and wettability to fulfill the functions. Especially, the MPLs are more hydrophobic in many cases to enable better water management for PEM fuel cells [24-26]. The GDLs are treated hydrophobic to avoid channel liquid water flows back and floods the electrode [27-29]. Figure 3 shows the schematic of water and thermal management in the cathode structure of a PEM fuel cell, water and heat need to be removed via GDLs from the catalyst layer [64].

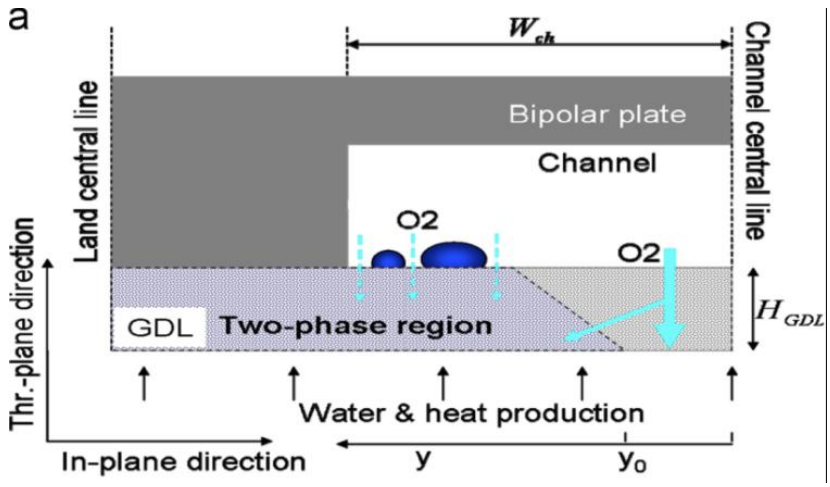

Figure 3 Schematic of water and thermal management in the cathode structure of a PEM fuel cell [64]

1.4 HEAT PIPE AND HEAT PIPE EFFECT

Most of the thermal diodes are manufactured based on the heat pipe principle, like thermal diode panels [30], plane-type bidirectional thermal diode [31], liquid-trap heat pipe thermal diode [32], and more. Heat Pipe shown in figure 4 is a vacuum-sealed metal tube that contains a working fluid that changes from liquid to gas when the heat is applied at one end of the tube. At the evaporation side, the liquid work fluid evaporates, absorbing heat. The resulting vapor trans- ports towards the condensation side, where the vapor condenses to liquid, releasing heat. The condensed work fluid then returns back to the evaporation side, restarting the cycle. In this process, heat is transported from the evaporation to the condensation sides. This design allows heat pipes to transfer heat much more efficiently than a solid piece of metal, and they have the added advantage of being much lighter. On top of that, modern heat pipe designs perform really well in any orientation, even upside down, that is why most high-performance CPU or graphics card coolers use heat pipe technology in some way these days.

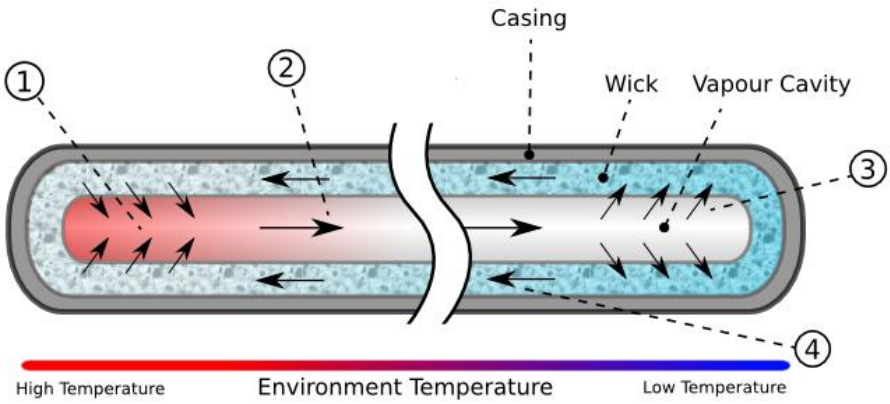

Heat pipe thermal cycle
1) Working fluid evaporates to vapour absorbing thermal energy.
2) Vapour migrates along cavity to lower temperature end.
3) Vapour condenses back to fluid and is absorbed by the wick, releasing thermal energy
4) Working fluid flows back to higher temperature end.

Figure 4. Heat pipe thermal cycle [33]

In PEM fuel cells, heat pipe effects occur due to water and heat generation in the electrodes, making the nonisothermal phenomena in fuel cells complex [34-37]. Wang and Wang [38-39] evaluated vapor-phase diffusion and heat pipe conductance, indicating that the former is a significant mechanism in the water management of PEM fuel cell and the latter contributes about 0.3–0.5 W/m °C conductivity at 80 °C. Wang and Mehernosh [40] used hydrophilic and hydrophobic carbon papers to measure the heat pipe effect. Figure 5 shows the schematics of heat transfer in a day carbon paper. Assuming the vapor diffusion is the limiting factor in heat pipe effect, the delivered heat flux can be estimated as follow:

$$h_{fg}\dot{m}_{fg} = h_{fg}M_w D_g^{w,eff}(T,P)\frac{dC_{sat}(T)dT}{dTdx} = k_{hp}(T,P)\frac{dT}{dx}$$

The above derivation indicates the heat pipe effect can be described using an apparent thermal conductivity k_{hp}. This conductivity is a function of temperature, pressure, and pore structure.

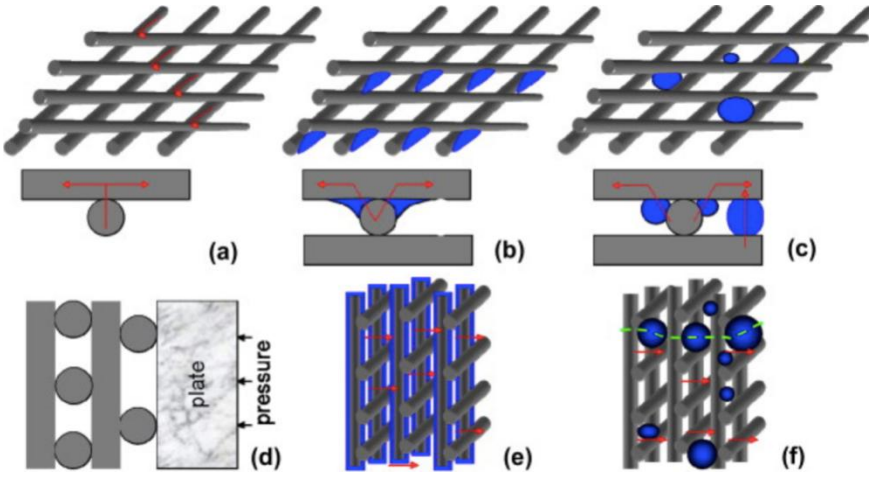

Figure 5 Schematics of heat transfer in a dry carbon paper. (a) Hydrophilic carbon paper. (b) Hydrophobic carbon paper. (c) The contacts between the sample and plate

and among fibers. (d) Heat flow by heat pipe effects in hydrophilic carbon paper. (e) Hydrophobic carbon paper. (f) The carbon fibers are intently drawn in a structural fashion for illustration purposes [40]

1.5 NOVEL THERMAL DIODE DESIGN FROM PEM FUEL CELL

Controlling the direction of heat transfer is important to various engineering applications such as power generation, cooling unit, thermal energy harvest, and hyperthermal treatment. Thermal diodes and thermal rectification units are two-terminal devices that enable heat transfer more easily in one direction than in the opposite direction, similar to the function of a standard diode on electric current control. These devices could be useful in a series of applications, especially in the fields that require proper thermal management. For example, for house thermal management, these devices could reduce the influx of heat from outside, and thus reduce the cooling load during the daytime. At night, they could dissipate heat quickly out of the house to make it more energy-efficient and environmentally friendly.

Most of the thermal diodes are manufactured based on the heat pipe principle. Now, many novel thermal diode devices were designed by exploiting new materials with unique thermal properties [41-43], such as phase change materials, shape memory alloys, phonon rectification membranes, and more. Ghanekar et al. [44] used the metal-insulator transition of VO_2 near 314 K to successfully design a near-field

thermal diode. This new material could achieve the thermal rectification ratio as high as 16 under a temperature difference of 20 K using 1-D triangular VO2 surface gratings. Pallecchi et al. [45] introduced a new thermal diode design based on a phase changing material poly(N-isopropylacrylamide) (PNIMA), which changes its hydrophilicity upon heating due to the phase separation of water from itself. At a temperature difference of 30 ˚C, the diodicity reached about 2~3. Schmotz et al. [46] built a novel thermal diode with a thin Si membrane, in which there was a rectification of heat flow carried by phonons. This thin layer could achieve a rectification ratio of the heat current of 1.7±0.2 at 150 K. These unique thermal diodes are thin with a thickness ranging from 100 nm to 10 micrometers. However, their study still stays at the laboratory level. Boreyko et al. [47] developed a vapor chamber thermal diode using water evaporation and coalescing-jumping droplets between a superhydrophobic surface and a superhydrophilic surface. The effects of thermal conductivity in the forward and reverse modes, as well as thermal rectification on the vapor chamber thermal diode in the gravitational anti-gravitational and the sideways directions, were investigated. In this diode, the superhydrophobic surface and the superhydrophilic surface were placed parallel and separated with a rubber gasket. The vapor space between the two plates was about 1.6 mm, and it was degassed to 3 kPa. Figure 6 shows the working principle of the vapor chamber thermal diode in the anti-gravitational direction. The superhydrophilic plate was heated in the forward mode, resulting in water vapor evaporation inside its wick structure. The superhydrophobic plate was cooled and used as a condenser of the

system. Due to low temperatures, water droplets were condensed and balled up on the superhydrophobic surface. Droplets coalesced with nearby droplets creating the jumping phenomenon. The coalescing-jumping droplets departed from the suerhydrophobic surface and returned to the wick structure in the superhydrophilic copper plate. In the reverse mode, the superhydrophobic surface was heated and its temperature was higher than that of the superhydrophilic copper plate. However, without any working fluid on the superhydrophobic surface, heat transfer took place mainly through the rubber gasket with high thermal resistance.

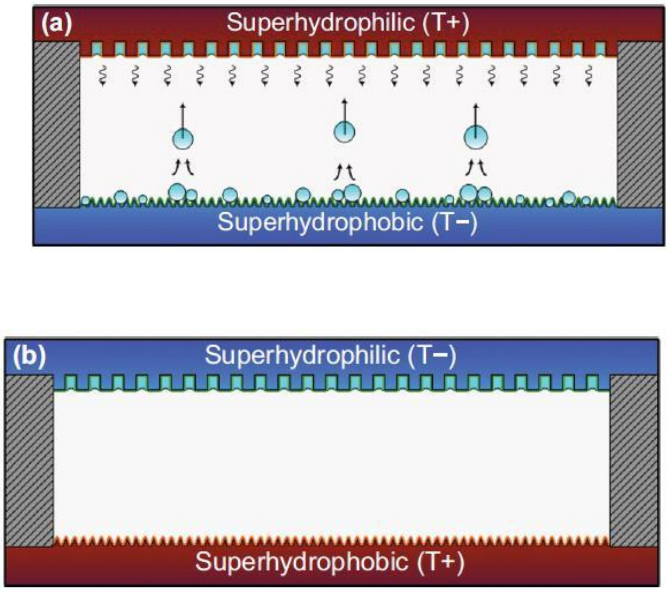

Figure 6. A schematic diagram of the vapor chamber thermal diode

In 2015, Wang [48] reported a novel thermal diode design by sandwiching two distinct layers and utilizing the heat pipe effect. The structure of diodes in this thesis is developed based on heterogeneous structures of either CL-MPL, MPL-GDL, or GDL-gas flow channels. The basic concept is one direction of heat removal and water removal from catalyst layers to the gas flow channels, like that in PEM fuel cells. The

diodes are thin at microscale thickness and flexible. In this thesis, an experiment was designed to fabricate a thermal diode layer following the concept and measure its thermal diodicity at room temperature and elevated conditions, respectively. Superhydrophobic materials are also tested, which are expected to have a strong impact on two-phase flow [49] and thus heat pipe effect. Different liquid contents are examined to explore their impacts on thermal performance.

CHAPTER 2 METHODS FOR THERMAL RESISTANCE MEASUREMENT

2.1 INTRODUCTION TO THERMAL RESISTANCE MEASUREMENT

Thermal resistance is a heat property and a measurement of a temperature difference by which an object or material resist a heat flow. Thermal resistance is the reciprocal of thermal conductivity, which measures the heat conducting capability of a material. As shown in figure 7a, it can be defined as the thermal energy (heat) Q transmitted through a length or thickness L, in the direction normal to a surface area A, under a steady-state temperature difference T_h-T_c. The resistance equals the length L divided by thermal conductivity k and area A. Interfacial thermal conductance (denoted as K or G) is defined as the ratio of heat flux to temperature drop across the interface of two components. For bulk materials, the temperature drop across an interface is

primarily due to the roughness of the surfaces because it is generally impossible to have “atomically smooth contact” at the interface as shown in figure 7b. Interfacial thermal conductance of bulk materials is affected by several factors such as surface roughness, surface hardness, impurities and cleanness, the thermal conductivity of the mating solids and the contact pressure [50]. For thin films, the temperature drop across aninterface can be attributed to the bonding strength and material difference. Note that thermal contact resistance and thermal boundary resistance (or Kapitza resistance [51]) are usually used to describe heat conduction capability of an interface in bulk materials and thin films, respectively. Interfacial thermal conductance is simply the inverse of thermal contact/boundary resistance. In this paper, we review measurement techniques for characterizing thermal resistance and interfacial thermal resistance of solid- state materials in both bulk and thin film forms.

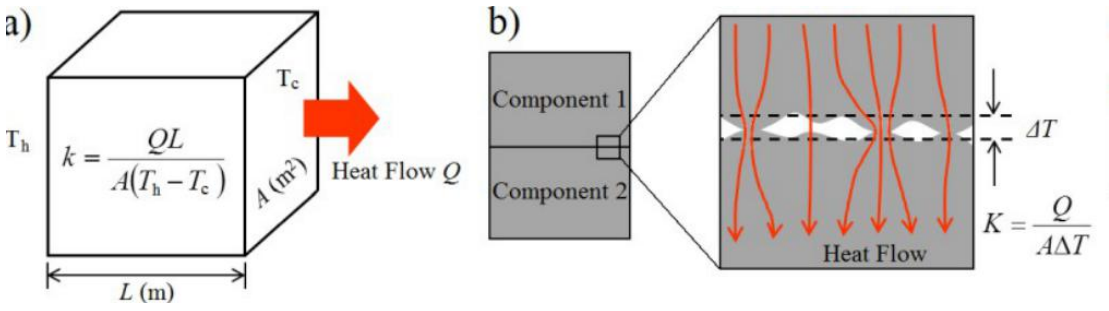

Figure 7. a) Definition of thermal conductivity of a solid bulk material using Fourier’s law of heat conduction. Temperature at the left and right sides are Th and Tc, respectively. Heat transfer cross- sectional area is denoted by A. The heat flow is assumed to be one-dimensional with no lateral heat loss. b) Definition of interfacial thermal conductance K at the contact between two bulk materials. Bulk materials are

contacted through limited contact points, which results in a temperature drop ΔT across the interface [50].

2.2 EXPERIMENTAL METHODS FOR THERMAL RESISTANCE MEASUREMENT

Extensive efforts have been made since the 1950s for the characterization of thermal conductivity and thermal contact resistance in bulk materials [52–57]. Table 1 summarizes some of the most commonly used measurement techniques, which in general can be divided into two categories: steady-state methods and transient methods. The steady-state methods measure thermal properties by establishing a temperature difference that does not change with time. Transient techniques usually measure the time-dependent energy dissipation process of a sample.

	Bulk material	**Thin film**
Steady-state	Absolute technique; Comparative technique; Radial heat flow method; Parallel conductance method	Steady-state electrical heating methods
Transient (frequency-domain)	Pulsed power technique	3ω method; FDTR technique

Transient (time-domain)	Hot-wire method (needle-probe method); Laser flash method; Transient plane source (TPS) method	TDTR technique

Table 1. Commonly used thermal characterization techniques

Each of these techniques has its own advantages and limitations, and is suitable for only a limited range of materials, depending on the thermal properties, sample configuration, and measurement temperature. Table 2 shows the material need of each method and their advantages and limitations [58-61].

Method	Materials	Positive	Negative
Guarded hot plate	Insulation Materials and solid, opaque, insulators	High accuracy, thermal conductivity range, temperature range	Time consuming measurement, low conductivity materials
Cylinder	Metals	Temperature range, simultaneous measurement of electrical	Time consuming measurement

		conductivity. accuracy	
Heat-flow meter	Insulation, plastics, glasses, ceramics Some metals, rocks, polymers	Simple construction and operation	Measurement uncertainly, relative measurement, Low conductivity materials
Comparative	Metals, ceramics, plastics	Simple construction and operation, thermal conductivity range	Measurement uncertainly, relative measurement
Direct heating	Metals Wires, rods, tubes of electrical conductors	Simple and fast measurements, simultaneous determination of electrical conductivity	Only electrically conducting materials

Pipe method	Solids calcium silicates, mineral and refractory fiber blankets	Temperature range	Specimen preparation, long measurement time

Table 2. Methods of measuring thermal resistance with material, positive and negative effects

2.3 EXPERIMENT METHOD AND SETUP IN THIS STUDY

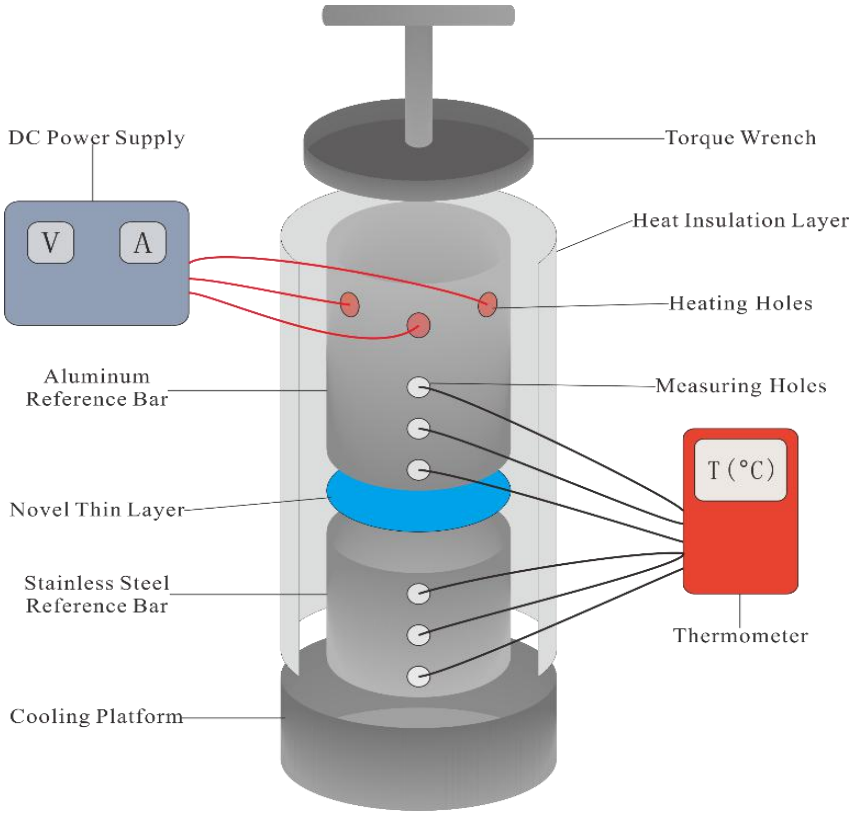

Figure 8. Schematic of the experimental setup for thermal resistance measurement

To measure the thermal resistance of the diode samples, the experiment was designed as shown in figure 8. The main body of the setup consists of one aluminum bar, one stainless steel bar, heating unit, cooling plate, insulation housing, and compression unit. Both metal bars have three small holes arranged in the axial direction, which provides sites to plug in thermocouple for temperature measurement. At the top of the aluminum bar, electric heating units were added to create a high temperature side, producing a conductive flow downwards towards the cooling base via the testing sample. A compression unit is mounted at the top to ensure identical pressure over samples during the testing. A heat insulation enclosure is added to the two bars and samples to reduce their heat loss through convection and radiation.

In the experiment, a sample is placed between the two metal bars. Six temperatures are measured and recorded when a steady state is reached, which usually takes about 1-2 hours. Each sample was measured under four different temperatures (60°C, 70°C, 80°C, 90°C) for both the conductive and opposite directions. For each case, six temperatures will be recorded for one thermal resistance measurement. The conductivity and the resistance are then calculated based on Fourier's law by the equation

$$Q = k\frac{\Delta T}{L}$$

$$R = \frac{L}{kA}$$

q: Heat flux (W/m^2)

R: Thermal resistance (K/W)

A: Area (m^2)

k: Thermal conductivity (W/mK)

ΔT: Temperature gradient (K)

d: Depth of conducting heat (m)

The heat flux q is determined by the heat fluxes through the two bars, which are calculated by the conductive flux using the known d between the holes and k of the metal bar. Note that the two fluxes are equal at stead state if the heat loss is negligible. The temperatures at the upper and lower surfaces of the sample are obtained by the extrapolation of the six recorded temperatures. The thermal resistance of a dry sample is the sum of the thermal resistances of two sublayers and the contact thermal resistances. As to wet samples, water and the heat pipe effect add into additional conductivity, as shown in Eq. 2:

$$k_{wet} - k_{dry} = \varepsilon^{\tau_l} k^l + k_{heat-pipe}$$

k_{wet}: thermal conductivity of wet layer (W/mK)

k_{dry}: thermal conductivity of dry layer (W/mK)

Ɛ: porosity of the material

$K_{heat\text{-}pipe}$: thermal conductivity of the heat pipe effect (W/mK)

CHAPTER 3 SAMPLE PREPARATION

3.1 SELECTION OF MATERIALS

A smart material whose heat conductivity/isolation could adjust to the external temperature changes would allow for the next generation of thermal diodes. Indeed, new materials whose thermal properties have been engineered are probably needed for a sustainable world. Pioneering work on solid state thermal diode based on nanomaterials has been demonstrated by Chang [62] using mass loaded nanotubes, and several studies on carbon based materials have been reported currently [63]. For uses that may lead to a real breakthrough in thermal management, either at the nano or large scale, novel solutions exploiting different materials are needed.

As introduced before, the thermal diode is assembled with a wet hydrophilic sublayer, a dry hydrophobic sublayer and the sealing material, as shown in figure 9.

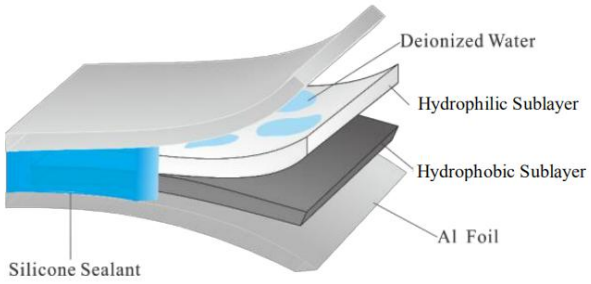

Figure 9. Ideal structure of the flexible micro-thickness thermal diode layer

Aluminum foil has a high thermal conductivity with 150 W/mK. Aluminum foil is also essentially impermeable to gases and water vapor. It can seal the water and gas inside of the thermal diodes. Therefore, Al foil is chosen for the sealing material because it is scarcely possible to influence the heat transfer of the thermal diodes.

The main parts of a thermal diode are the hydrophilic sublayer and the hydrophobic sublayer. Hydrophilic materials are easy to find, so printing paper and cellulose paper

(filter paper) were chosen because they are normal in the lab. Hydrophilic materials do not play an important role in heat pipe effect as long as the hydrophilic sublayer can absorb enough liquid. As Wang illustrated that the heat pipe effect is active in a part of the hydrophobic carbon paper, yielding a reduced increase in added thermal conductivity with temperature [40]. Carbon paper and printing paper was chosen as the hydrophobic sublayer and hydrophilic sublayer for the test sample of a thermal diode. Then facial masks made by polypropylene appear in the lab, and they are water-repellent. Polypropylene became the second hydrophobic material for a thermal diode to test.

3.2 SAMPLE PREPARATION PROCEDURE

Figure 10. Ideal flexible diode layer sample

The ideal flexible diode layer at first was assembled following the method, which consists of a hydrophobic sublayer and a wet hydrophilic sublayer sandwiched by two aluminum foil, as shown in Fig. 10. The internal structure is sealed using packaging tape to create a closed system for water phase change and flow, which transfers heat flow through the heat pipe effect. However, there was leakage of air after vacuuming. The packaging tape was changed to a circular ring with a water-proof silicone sealant. Built a sample and tested the leakage after vacuuming, only one to two bubbles appeared after putting the sample into a cup of water. Figure 11 shows the updated structure of the flexible micro-thickness thermal diode layer, and figure 12 shows the actual sample of printing paper and carbon paper.

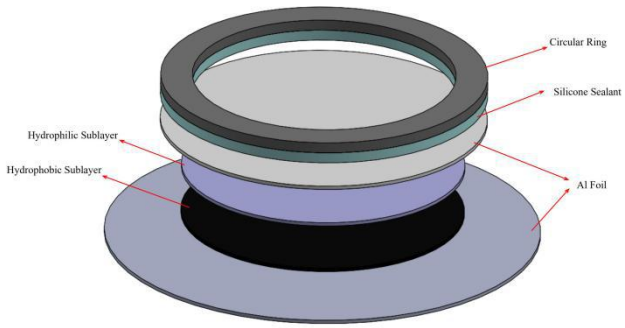

Figure 11. Structure of the flexible micro-thickness thermal diode layer with a hydrophobic layer and a wet hydrophilic layer sandwiched by two piece of foils

Figure 12. Actual sample of printing paper and carbon paper

Given that liquid working fluid is only permitted to flow to the hydrophilic part, the heat pipe conductance is only effective in one direction only, and will be inactive in the opposite direction. In the direction from the hydrophilic sublayer to the hydrophobic layer side, heat pipe flow is enabled by heat pipe, and thus labeled as 'hydrophilic direction'. In the opposite direction, heat is transferred through conduction primarily via the solid matrix. The Al foil is 50 micrometers thick, which yields the entire diode layer around 300 micrometers. Meanwhile, to study the influence of water content, two different samples were made with various water loadings, including 40 wt% water content samples and 60 wt% samples.

3.3 MATERIAL CHARACTERIZATION

3.3.1 PRINTING PAPER

Printing papers are the most common paper using for printing. They are also the most common hydrophilic materials. In this paper, the width of a printing paper is 0.1mm,

and the thermal conductivity of the printing paper is 0.05 W/m K, and the dynamic contact angle of a water droplet on carbon paper is 73.2˚ showed in figure 13. Figure 14 (d) also showed the microstructure of the printing paper used in this paper.

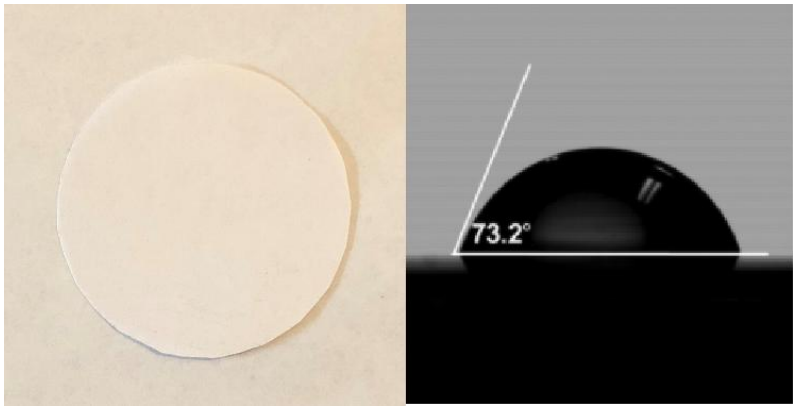

Figure 13. Liquid water droplets at the surfaces of the printing paper

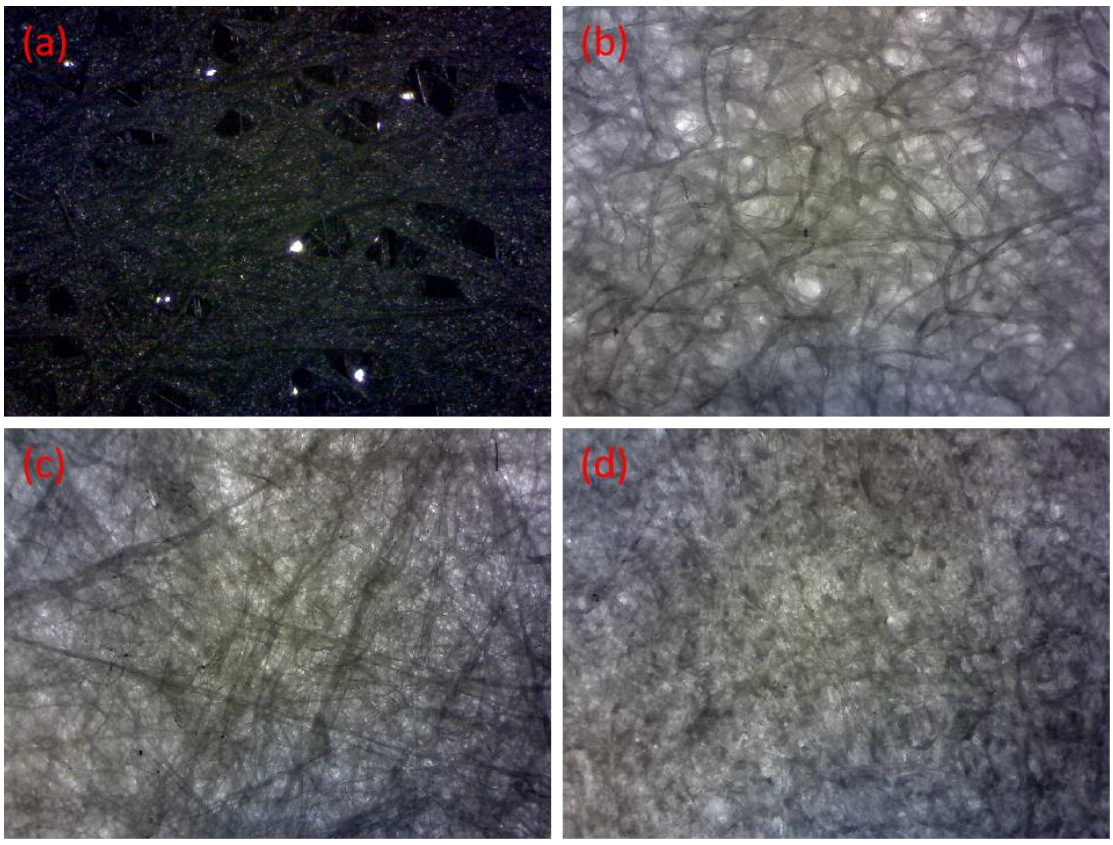

Figure 14. (a) Magnification of carbon paper. (b) Magnification of cellulose paper. (c) Magnification of polypropylene paper. (d) Magnification of printing paper

3.3.2 CARBON PAPER

Carbon papers are porous materials that are widely applied in a variety of engineering applications, such as batteries, heat transfer devices, fuel cells, multi-stage filters, high-temperature thermal insulators, and friction/wear applications. Carbon papers are non woven fibrous media, based on carbon fibers, and are commercially available. Thermal conductivity is an important property of carbon papers, particularly in thermal and power applications. Though carbon fibers are highly conductive, the effective conductivity can be low when the porosity is high. In this paper, the width of carbon paper is 0.19mm, and the thermal conductivity of the carbon paper is 0.55 W/m K, and the dynamic contact angle of a water droplet on carbon paper is 128˚ showed in figure 15. Figure 14 (a) also showed the microstructure of the carbon paper used in this paper and figure 16 showed the SEM image.

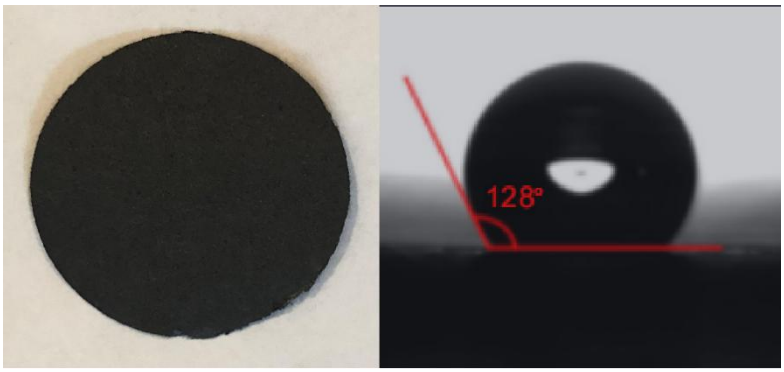

Figure 15. Liquid water droplets at the surfaces of the carbon paper

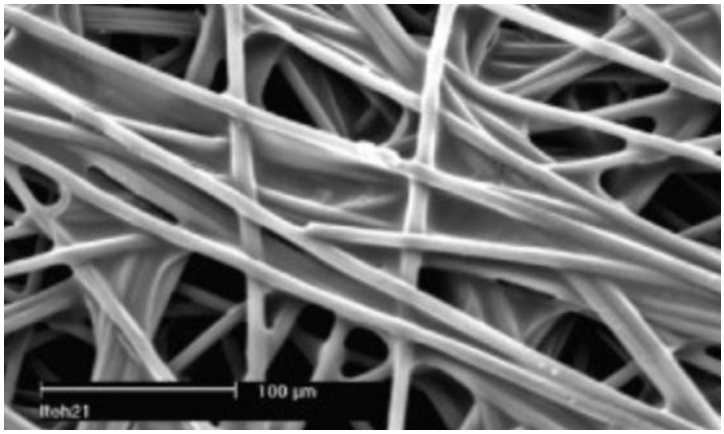

Figure 16. SEM image of carbon paper

3.3.3 CELLULOSE PAPER (FILTER PAPER)

Cellulose paper is a kind of membrane filters, which are polymer films with specific pore ratings. In this paper, the cellulose paper is composed of cellulose di- and triacetate. These materials exhibit low static charge and high strength. The width of cellulose paper is 0.19mm, and the thermal conductivity of the cellulose paper is 0.3 W/m K, and the dynamic contact angle of a water droplet on carbon paper is 55.2˚ showed in figure 17. Figure 14 (b) also showed the microstructure of the cellulose paper used in this paper.

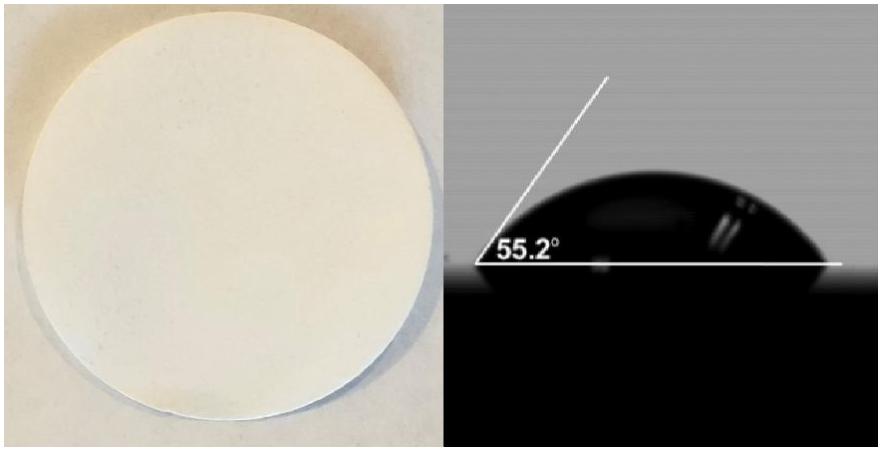

Figure 17. Liquid water droplets at the surfaces of the cellulose paper

3.3.4 POLYPROPYLENE PAPER

Polypropylene paper is the raw material of masks. This kind of materials is super hydrophobic in order to prevent virus. In this paper, the width of the polypropylene paper is 0.09mm, and the thermal conductivity of the carbon paper is 0.2 W/m K, and the dynamic contact angle of a water droplet on carbon paper is 102˚ showed in figure 18. Figure 14 (c) also showed the microstructure of the carbon paper used in this paper.

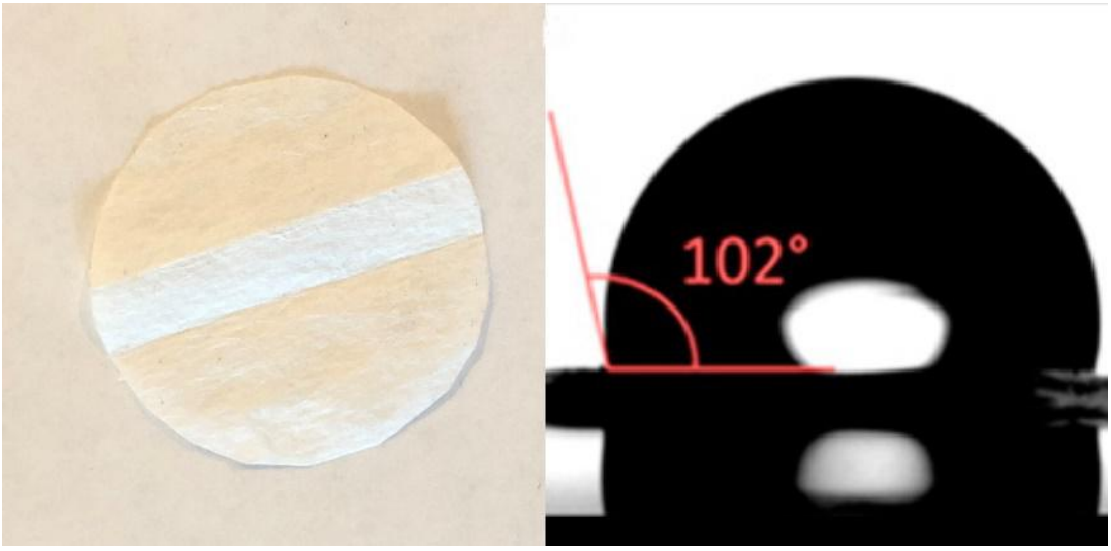

Figure 18. Liquid water droplets at the surfaces of the polypropylene paper

CHAPTER 4 RESULT AND DISCUSSION

4.1 PRINTING PAPER & CARBON PAPER

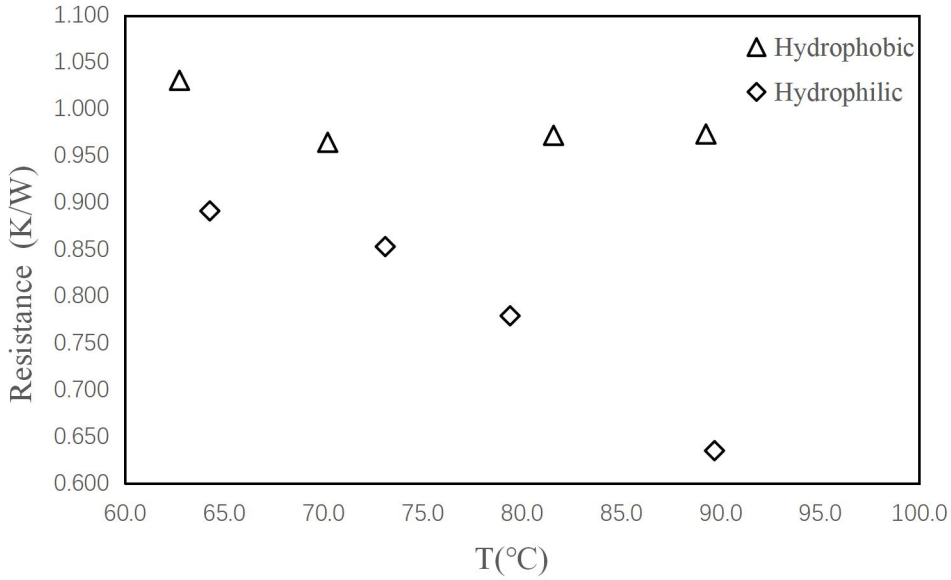

Figure 19. Thermal resistance of the diodes of 10% water load for printing paper & carbon paper

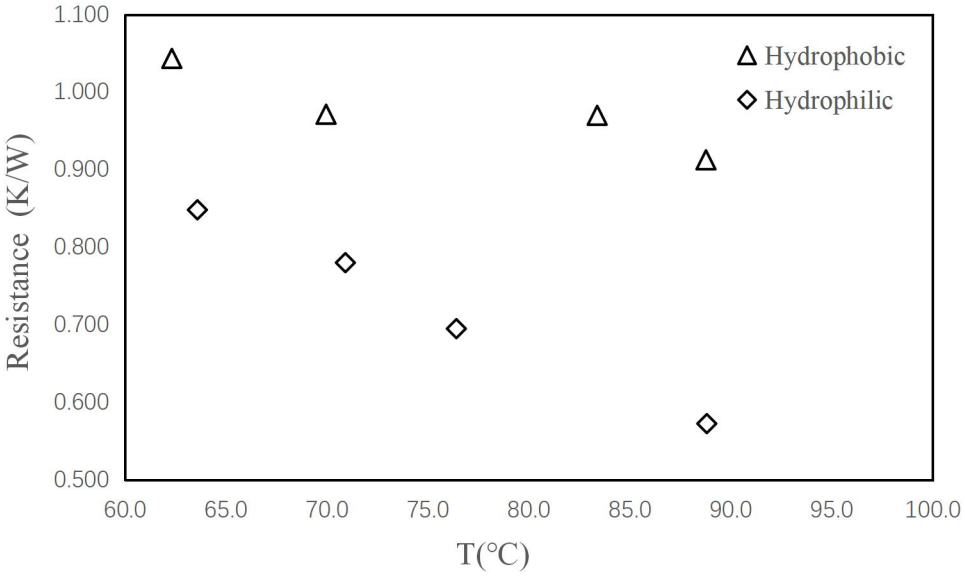

Figure 20. Thermal resistance of the diodes of 20% water load for printing paper & carbon paper

Printing paper and carbon paper was chosen to be the first sample to test the theory stated before. Figure 19 and figure 20 show thermal resistances measured for diodes of low water content under various temperatures. It is shown that the thermal

resistances have different trends in the two opposite directions. In the hydrophilic direction, i.e. the printing paper sublayer is closer to the heat source, thermal resistance decreases remarkably with temperature, and the decreasement is greater under higher temperatures. For the water content of 20%, the values are 0.848 K/W and 0.573 K/W at 60 °C and 90 °C, respectively, showing about 50% decrease. The same trend is observed for the 10% water content as well with the values being 0.891 K/W, 0.779 K/W, and 0.635 K/W at 60 °C, 80°C, and 90 °C , respectively. As to the hydrophobic direction, no significant change is observed among different temperatures. Meanwhile, compare with the different heated direction, the thermal resistance difference appears. That means the method used in this paper worked.

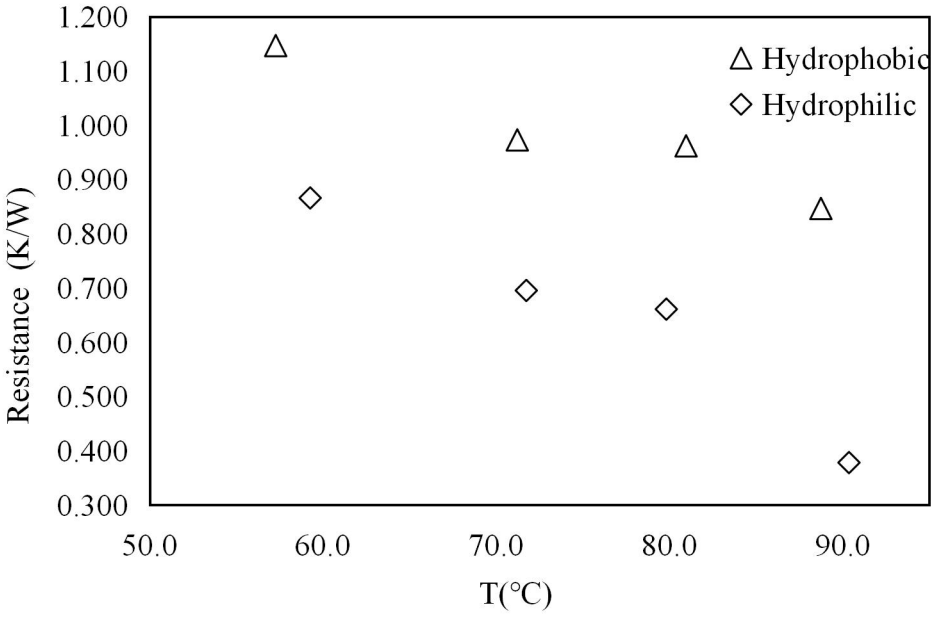

Figure 21. Thermal resistance of the diodes of 40% water load for printing paper & carbon paper

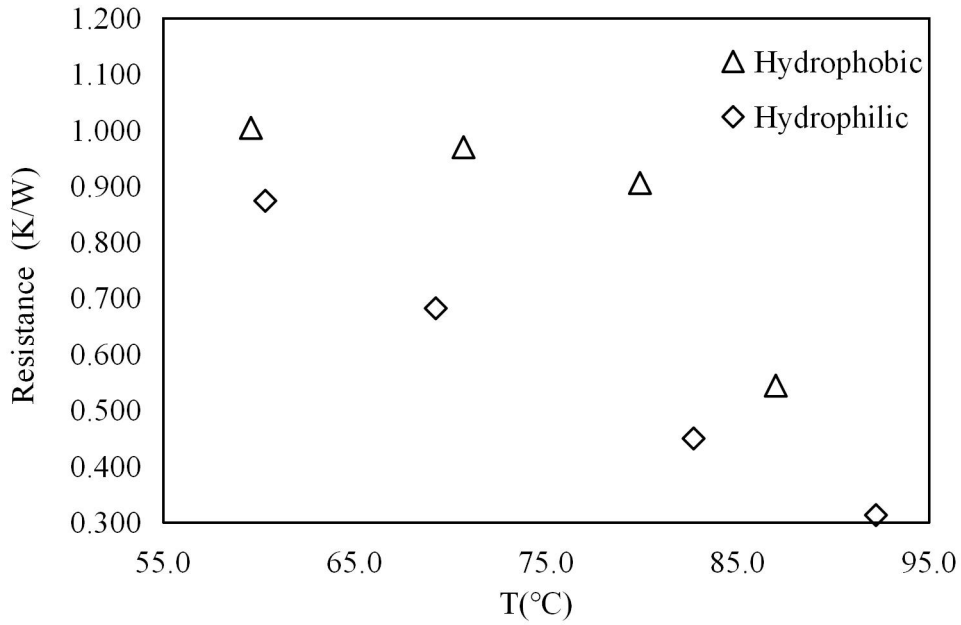

Figure 22. Thermal resistance of the diodes of 60% water load for printing paper & carbon paper

Figure 21 and figure 22 present the thermal resistances measured for diodes under high water contents of 40% and 60%. For the former, the trend of thermal resistance change with temperature is similar to that under low water contents. In the hydrophilic direction, the resistance shows a clear decrease with temperature, but not in the hydrophobic direction where the change is negligible. It is also shown that the resistance decrement is larger than the other two low content cases. At 90 °C, the measurement is 0.378 K/W, in comparison with only 0.866 K/W at 60 °C. The decreased resistance is 0.488 W/m K, about 130% decrease. Compare to low water contents, there are only about 50% decrease. As water adds to 60% in content, the trend of resistance change is totally different from the other three water contents. In the hydrophilic direction, the measurements are much smaller than the others. It reaches 0.874 K/W and 0.312 K/W at 60 °C and 90 °C, respectively. There is about

180% decrease. Meanwhile, in the opposite direction, the values are smaller than the others, which is about 0.7 W/m K versus about 0.95 W/m K for the others. It shows that the thermal resistance differences are proportional to water contents. Therefore, only high water content samples were made for other materials.

Comparing the hydrophobic direction and hydrophilic direction, the difference of thermal resistance at the same temperature shows the effect thermal diodes. For this sample diode, at 90 °C, the thermal resistance is 0.378 K/W at hydrophilic direction versus 0.847 K/W at the hydrophobic direction, about 125% decrease. As water adds to 60% in content, the thermal resistance is 0.312 K/W at hydrophilic direction versus 0.544 K/W at the hydrophobic direction, also about two times smaller. The goal is to find more conductive hydrophilic materials and less conductive hydrophobic materials to make the thermal diode perform higher efficiency.

4.2 CELLULOSE PAPER & CARBON PAPER

The dynamic contact angle of a water droplet on the cellulose paper is 55.2˚, and the thermal conductivity of cellulose paper is about 0.3 W/m K. Compare to the printing paper, the dynamic contact angle of a water droplet on printing paper is 73.2˚, and the thermal conductivity is about 0.05 W/m K. Cellulose paper is supposed to be a little bit better than printing paper when the water content is high.

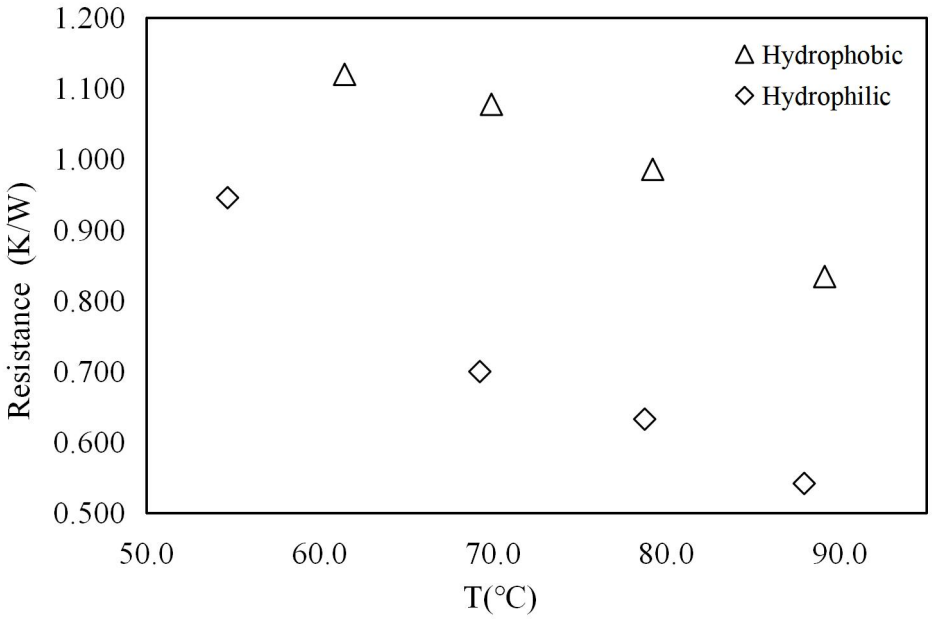

Figure 23. Thermal resistance of the diodes of 40% water load for cellulose paper & carbon paper

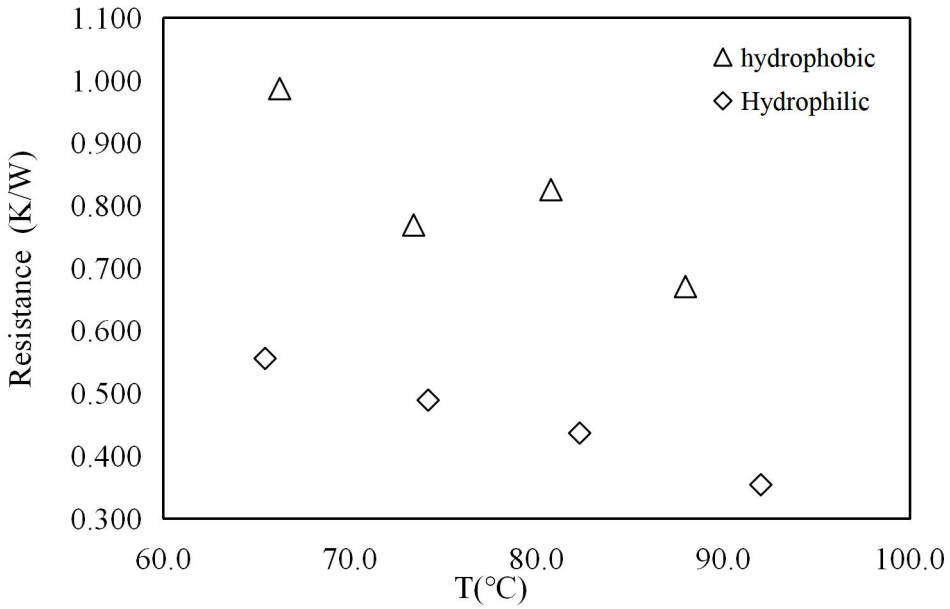

Figure 24. Thermal resistance of the diodes of 60% water load for cellulose paper & carbon paper

Figure 23 and figure 24 show the thermal resistance measured for diodes of cellulose paper and carbon paper under various temperatures. For the diodes of 40% water load,

the lowest thermal resistance is 0.541 K/W at the hydrophilic direction and 0.834 K/W at the hydrophobic direction. The difference is not much obvious than the printing paper sample, however, as water adds to 60% in content, it shows a better result. The thermal resistance of the hydrophilic direction are 0.354 K/W at 90°C and 0.556 K/W at 60°C, respectively. In the hydrophobic direction, the values are 0.671 K/W at 90°C and 0.987 K/W at 60°C. There is about 100% decrease between two directions. Compare to the printing paper sample with about 75% decrease, the sample of cellulose paper and carbon paper shows a better efficiency.

4.3 CELLULOSE PAPER & POLYPROPYLENE PAPER

After tried to change the hydrophilic material, hydrophobic materials are also considered to change to less conductive. For the carbon paper introduced before, the dynamic contact angles of a water droplet on carbon paper is 128˚, and the thermal conductivity is about 0.55 W/m K. While for the polypropylene paper, the dynamic contact angle of a water droplet on polypropylene paper is 102˚, and the thermal conductivity is about 0.2 W/m K. Based on the thermal conductivity of two materials, polypropylene paper should be better than carbon paper as the hydrophobic material in thermal diodes.

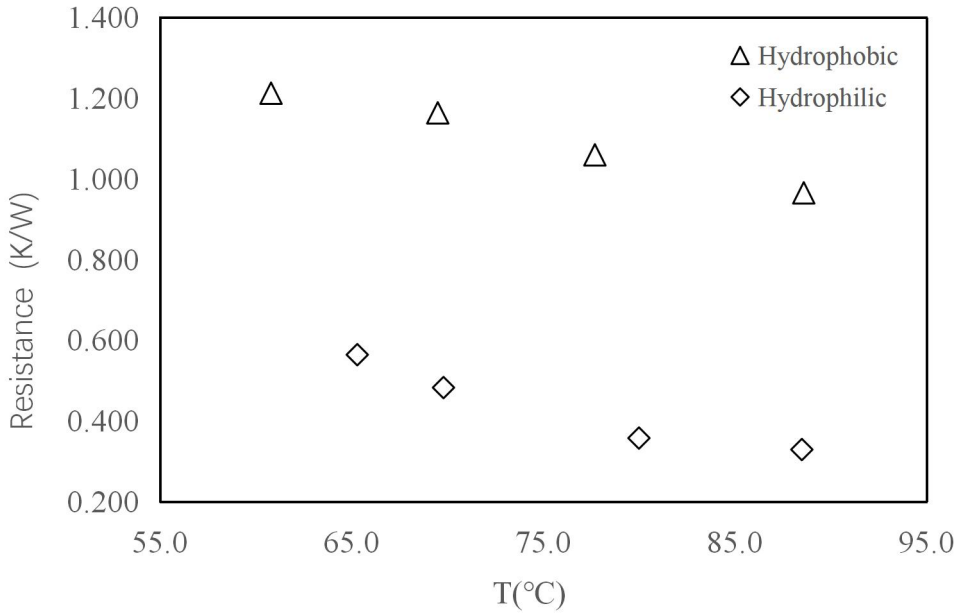

Figure 25. Thermal resistance of the diodes of 40% water load for cellulose paper & polypropylene paper

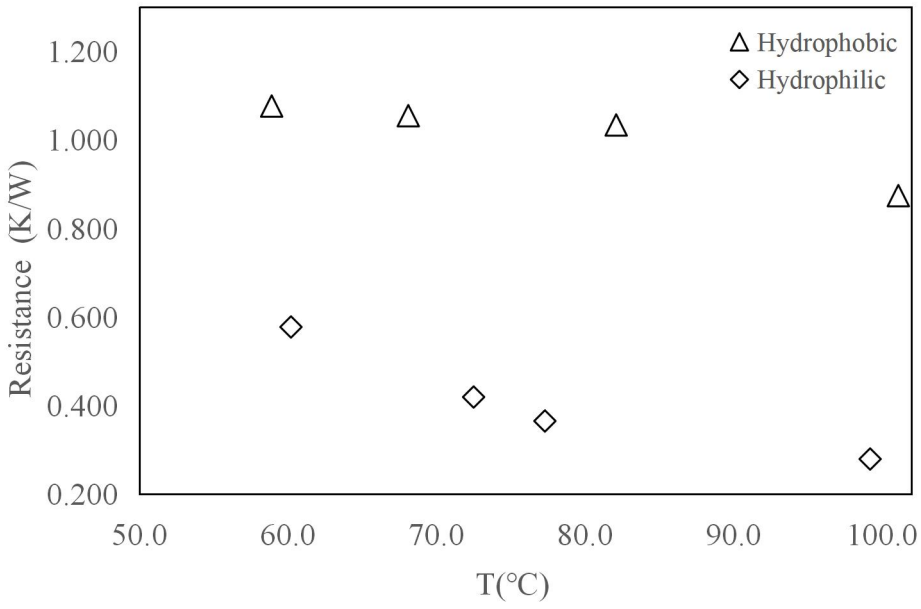

Figure 26. Thermal resistance of the diodes of 60% water load for cellulose paper & polypropylene paper

Figure 25 and figure 26 show the thermal resistances measured for diodes of cellulose paper and polypropylene paper under various temperatures. For the diodes of 40%

water load, the lowest thermal resistance is 0.329 K/W at the hydrophilic direction and 0.965 K/W at the hydrophobic direction, about a 193% increase. Even at 60℃, the thermal resistance is 0.564 K/W at the hydrophilic direction and 1.212 K/W at the hydrophobic direction, over two times larger. As water adds to 60% in content, the lowest thermal resistance becomes 0.28 K/W at the hydrophilic direction and 0.874 K/W at the hydrophobic direction, about 210% increase. At 60℃, the thermal resistance is 0.578 K/W at hydrophilic direction and 1.077 K/W at hydrophobic direction, also about two times larger. Therefore, a thermal diode with cellulose paper and polypropylene paper can produce a 2-3 times difference between hydrophilic direction and hydrophobic direction based on temperature. Compared to the carbon paper and cellulose paper sample, the sample of polypropylene and cellulose papers shows a large improvement.

CHAPTER 5 CONCLUSION

This study presented an experimental study of the thermal resistances of microscale-thick thermal diodes based on PEM fuel cell structure, which consist of a wet hydrophilic layer and a nonwetting hydrophobic layer. The thermal measurement is based on Fourier's law, which measured six temperatures in the two metal bars to calculate the heat flux and the surface temperatures of the testing sample. Measurement was conducted under different temperatures and water contents to explore the thermal resistance as a function of these important parameters. Printing paper and cellulose paper (Filter paper) are used as hydrophilic materials, while carbon paper (a contact angle of 128˚) and polypropylene paper (with a contact angle of 102˚) are used as hydrophobic materials. The below are the major findings:

For the printing paper and carbon paper structure: in one direction, the resistance varies from 0.866 K/W to 0.378 K/W at the water content of 40% and 0.874 K/W to 0.312 K/W at the water content of 60% as temperature increases from 60°C to 90°C. In the other direction, the resistance varies from 1.147 K/W to 0.847 K/W at the water content of 40% and 1.004 K/W to 0.544 K/W at the water content of 60%. A maximum of about two times difference diodicity was achieved.

For cellulose paper and carbon paper: in one direction, the resistance varies from 0.945 K/W to 0.541 K/W at the water contents of 40% and 0.556 K/W to 0.354 K/W at the water contents of 60% as temperature increases from 60°C to 90°C. In the other direction, the resistance varies from 1.12 K/W to 0.834 K/W at the water contents of

40% and 0.987 K/W to 0.671 K/W at water contents of 60%. A maximum of about two times difference diodicity was achieved.

For cellulose paper and polypropylene paper: in one direction, the resistance varies from 0.564 K/W to 0.329 K/W at the water contents of 40% and 0.578 K/W to 0.28 K/W at the water contents of 60% as temperature increases from 60°C to 90°C. In the other direction, the resistance varies from 1.212 K/W to 0.965 K/W at the water contents of 40% and 1.077 K/W to 0.874 K/W at the water contents of 60%. A maximum of about three times difference diodicity was achieved.

Under high temperature, the heat pipe effect becomes significant, decreased the overall thermal resistance of the thermal diode. The decreased resistance decreases rapidly with temperature with about 0.6 K/W maximum from 60 °C to 90 °C.

Under high water content, heat pipe effect also becomes active, decreased the overall thermal resistance of the thermal diode. The decreased resistance decreases rapidly with water contents with about 0.4 K/W maximum from 40% water load to 60% water load.

REFERENCE

1. Incropera, Frank P., et al. Principles of Heat and Mass Transfer. John Wiley & Sons Singapore Pte. Ltd., 2014.
2. “Heat Transfer¶.” Heat Transfer - Introduction to Chemical and Biological Engineering, www.engr.colostate.edu/CBE101/topics/heat_transfer.html.
3. Wang, Yun, et al. “A Review of Polymer Electrolyte Membrane Fuel Cells: Technology, Applications, and Needs on Fundamental Research.” Applied Energy, vol. 88, no. 4, 2011, pp. 981–1007., doi:10.1016/j.apenergy.2010.09.030.
4. Song, G. H., & Meng, H. (2013). Numerical modeling and simulation of PEM fuel cells: Progress and perspective. Acta Mechanica Sinica, 29(3), 318-334.
5. Wu, H. W. (2016). A review of recent development: Transport and performance modeling of PEM fuel cells. Applied Energy, 165, 81-106.
6. Wang, Y., Diaz, D. F. R., Chen, K. S., Wang, Z., & Adroher, X. C. (2020). Materials, technological status, and fundamentals of PEM fuel cells–a review. Materials Today, 32, 178-203.
7. Demuren, A., & Edwards, R. L. (2020). Modeling Proton Exchange Membrane Fuel Cells—A Review. In 50 Years of CFD in Engineering Sciences (pp. 513-547). Springer, Singapore.
8. Newman, J., & Thomas-Alyea, K. E. (2012). Electrochemical systems. John Wiley & Sons

9. “Fuel Cell Technologies Office Multi-Year Research, Development, and Demonstration Plan.” Energy.gov, www.energy.gov/eere/fuelcells/downloads/fuel-cell-technologies-office-multi-year-research-development-and-22.
10. Wang, Yun, et al. “Fundamentals, Materials, and Machine Learning of Polymer Electrolyte Membrane Fuel Cell Technology.” Energy and AI, vol. 1, 2020, p. 100014., doi:10.1016/j.egyai.2020.100014.
11. Wang, Y., & Feng, X. (2009). Analysis of the reaction rates in the cathode electrode of polymer electrolyte fuel Cells: II. Dual-Layer electrodes. Journal of The Electrochemical Society, 156(3), B403.
12. Liu, X., Peng, F., Lou, G., & Wen, Z. (2015). Liquid water transport characteristics of porous diffusion media in polymer electrolyte membrane fuel cells: A review. Journal of Power Sources, 299, 85-96.
13. Sun, P. (2012). Efficient numerical methods for an anisotropic, nonisothermal, two-phase transport model of proton exchange membrane fuel cell. Acta applicandae mathematicae, 118(1), 251-279.
14. Wang, Y. (2009). Porous-Media Flow Fields for Polymer Electrolyte Fuel Cells: I. Low Humidity Operation. Journal of The Electrochemical Society, 156(10), B1124.
15. Wang, Yun, et al. PEM Fuel Cells: Thermal and Water Management Fundamentals. Momentum Press, 2013.

16. Benner, J., Mortazavi, M., & Santamaria, A. D. (2018, November). Numerical Simulation of Droplet Emergence and Growth From Gas Diffusion Layers (GDLs) in Proton Exchange Membrane (PEM) Fuel Cell Flow Channels. In ASME 2018 International Mechanical Engineering Congress and Exposition. American Society of Mechanical Engineers Digital Collection.
17. Ko, J., & Ju, H. (2012). Comparison of numerical simulation results and experimental data during cold-start of polymer electrolyte fuel cells. Applied energy, 94, 364-374.
18. Wan, Z., Chang, H., Shu, S., Wang, Y., & Tang, H. (2014). A review on cold start of proton exchange membrane fuel cells. Energies, 7(5), 3179-3203.
19. Ko, J., & Ju, H. (2013). Effects of cathode catalyst layer design parameters on cold start behavior of polymer electrolyte fuel cells (PEFCs). international journal of hydrogen energy, 38(1), 682-691.
20. Mishler, J., Wang, Y., Mukherjee, P. P., Mukundan, R., & Borup, R. L. (2012). Subfreezing operation of polymer electrolyte fuel cells: ice formation and cell performance loss. Electrochimica Acta, 65, 127-133.
21. Carrere, P., & Prat, M. (2019). Impact of non-uniform wettability in the condensation and condensation-liquid water intrusion regimes in the cathode gas diffusion layer of proton exchange membrane fuel cell. International Journal of Thermal Sciences, 145, 106045.

22. Adroher, X. C., & Wang, Y. (2011). Ex situ and modeling study of two-phase flow in a single channel of polymer electrolyte membrane fuel cells. Journal of Power Sources, 196(22), 9544-9551.
23. Macauley, N., Lujan, R. W., Spernjak, D., Hussey, D. S., Jacobson, D. L., More, K., ... & Mukundan, R. (2016). Durability of polymer electrolyte membrane fuel cells operated at subfreezing temperatures. Journal of The Electrochemical Society, 163(13), F1317-F1329.
24. Sun, P. (2012). A domain decomposition method for a two-phase transport model of polymer electrolyte fuel cell containing micro-porous layer. International journal for numerical methods in engineering, 91(10), 1115-1136
25. Niblett, D., Mularczyk, A., Niasar, V., Eller, J., & Holmes, S. (2020). Two-phase flow dynamics in a gas diffusion layer-gas channel-microporous layer system. Journal of Power Sources, 471, 228427.
26. Cho, J., Park, J., Oh, H., Min, K., Lee, E., & Jyoung, J. Y. (2013). Analysis of the transient response and durability characteristics of a proton exchange membrane fuel cell with different micro-porous layer penetration thicknesses. Applied energy, 111, 300-309
27. Carrere, P., & Prat, M. (2019). Impact of non-uniform wettability in the condensation and condensation-liquid water intrusion regimes in the cathode gas diffusion layer of proton exchange membrane fuel cell. International Journal of Thermal Sciences, 145, 106045.

28. Niu, Z., Bao, Z., Wu, J., Wang, Y., & Jiao, K. (2018). Two-phase flow in the mixed-wettability gas diffusion layer of proton exchange membrane fuel cells. Applied Energy, 232, 443-450.

29. Park, J., Oh, H., Lee, Y. I., Min, K., Lee, E., & Jyoung, J. Y. (2016). Effect of the pore size variation in the substrate of the gas diffusion layer on water management and fuel cell performance. Applied Energy, 171, 200-212.

30. Varga, Szabolcs, Armando C Oliveira, and Clito F Afonso. "Characterisation of Thermal Diode Panels for Use in the Cooling Season in Buildings." Energy & Buildings 34.3 (2002): 227–235. Web.

31. Chen, K, and Univ. of Utah Dept. of Mechanical and Industrial Engineering. "Design of a Plane-Type Bidirectional Thermal Diode." J. Sol. Energy Eng.; (United States) 110.4 (1988): 299–305. Web.

32. Groll, M et al. "Development of a Liquid-Trap Heat Pipe Thermal Diode." Journal of Spacecraft and Rockets 16.4 (1979): 195–202. Web.

33. Vanyasree, G., and P.V. Ramana. "EXPERIMENTAL ANALYSIS ON THERMOSYPHON HEATPIPE TO FIND HEAT TRANSFER COEFFICENT." International Research Journal of Engineering and Technology (IRJET), vol. 04, no. 08, Aug. 2017.

34. Ge, N., Chevalier, S., Lee, J., Yip, R., Banerjee, R., George, M. G., ... & Kotaka, T. (2017). Non-isothermal two-phase transport in a polymer electrolyte membrane fuel cell with crack-free microporous layers. International Journal of Heat and Mass Transfer, 107, 418-431.

35. Markötter, H., Manke, I., Kuhn, R., Arlt, T., Kardjilov, N., Hentschel, M. P., ... & Banhart, J. (2012). Neutron tomographic investigations of water distributions in polymer electrolyte membrane fuel cell stacks. Journal of Power Sources, 219, 120-125.

36. Wang, Y., Pham, L., de Vasconcellos, G. P. S., & Madou, M. (2010). Fabrication and characterization of micro PEM fuel cells using pyrolyzed carbon current collector plates. Journal of Power Sources, 195(15), 4796-4803.

37. Fadzillah, D. M., Rosli, M. I., Talib, M. Z. M., Kamarudin, S. K., & Daud, W. R. W. (2017). Review on microstructure modelling of a gas diffusion layer for proton exchange membrane fuel cells. Renewable and sustainable energy reviews, 77, 1001-1009.

38. Y. Wang, C.Y. Wang, A non-isothermal, two-phase model for polymer electrolyte fuel cells, J. Electrochem. Soc. 153 (2006) A1193–A1200.

39. Y. Wang, C.Y. Wang, Two-phase transients of polymer electrolyte fuel cells, J. Electrochem. Soc. 154 (2007) B636–B643.

40. Wang, Y., & Gundevia, M. (2013). Measurement of thermal conductivity and heat pipe effect in hydrophilic and hydrophobic carbon papers. International Journal of Heat and Mass Transfer, 60, 134-142. doi:10.1016/j.ijheatmasstransfer.2012.12.016

41. Pallecchi, E et al. “A Thermal Diode and Novel Implementation in a Phase-Change Material.” Materials Horizons 2.1 (2014): 125–129. Web.

42. Tso, C.Y, and Christopher Y.H Chao. “Solid-State Thermal Diode with Shape Memory Alloys.” International Journal of Heat and Mass Transfer 93 (2016): 605–611. Web.
43. Schmotz, Markus et al. “Athermal Diode Using Phonon Rectification.” New Journal of Physics 13.11 (2011): 8. Web.
44. Ghanekar, A et al. “Near-Field Thermal Rectification Devices Using Phase Change Periodic Nanostructure.” Optics Express 26.2 (2018): A209–A218. Web.
45. Pallecchi, E. et al. “A Thermal Diode and Novel Implementation in a Phase-Change Material.” Materials Horizons 2.1 (2015): 125–129. Web.
46. Schmotz, M. et al. “A thermal Diode Using Phonon Rectification.” New Journal of Physics 13.11 (2011): 8. Web.
47. J. Boreyko, Y. Zhao and C. Chen, “Planar jumping-drop thermal diodes,” Applied Physics Letters, vol. 99, p. 234105, 2011.
48. Wang, Y. Thermal Devices For Controlling Heat Transfer. 13 Aug. 2015.
49. Randive, P., Dalal, A., & Mukherjee, P. P. (2014). Probing the influence of superhydrophobicity and mixed wettability on droplet displacement behavior. Microfluidics and nanofluidics, 17(4), 657-674.
50. Savija, I., Culham, J. R., Yovanovich, M. M. & Marotta, E. E. Review of thermal conductance models for joints incorporating enhancement materials. J. Thermophys. Heat Transf. 17, 43–52 (2003).
51. Pollack, G. L. Kapitza Resistance. Rev. Mod. Phys. 41, 48–81 (1969).

52. Tritt, T. M. & Weston, D. in Thermal Conductivity (ed. Tritt, T. M.) 187–203 (Springer US, 2004).

53. Hamilton, R. L. & Crosser, O. K. Thermal conductivity of heterogeneous two-component systems. Ind. Eng. Chem. Fundam. 1, 187–191 (1962).

54. Zeller, R. C. & Pohl, R. O. Thermal Conductivity and Specific Heat of Noncrystalline Solids. Phys. Rev. B 4, 2029–2041 (1971).

55. Cooper, M. G., Mikic, B. B. & Yovanovich, M. M. Thermal contact conductance. Int. J. Heat Mass Transf. 12, 279–300 (1969).

56. Madhusudana, C. V. & Fletcher, L. S. Contact heat transfer - The last decade. AIAA J. 24, 510–523 (1986).

57. Prasher, R. Thermal Interface Materials: Historical Perspective, Status, and Future Directions. Proc. IEEE 94, 1571–1586 (2006).

58. He, Yi. “Rapid Thermal Conductivity Measurement with a Hot Disk Sensor.” Thermochimica Acta 436.1 (2005): 130–134. Web.

59. Cha, Junghoon, Jungki Seo, and Sumin Kim. “Building Materials Thermal Conductivity Measurement and Correlation with Heat Flow Meter, Laser Flash Analysis and TCi.” Journal of Thermal Analysis and Calorimetry 109.1 (2012): 295–300. Web.

60. Sidorov, Anton N., Daniel K. Benjamin, and Christopher Foy. “Comparative Thermal Conductivity Measurement of Chemical Vapor Deposition Grown Graphene Supported on Substrate.” Applied Physics Letters 103.24 (2013): . Web.

61. Zhao, Dongliang et al. “Measurement Techniques for Thermal Conductivity and Interfacial Thermal Conductance of Bulk and Thin Film Materials.” arXiv.org 138.4 (2016): n. pag. Web.

62. C. W. Chang, D. Okawa, A. Majumdar and A. Zettl, *Science*, 2006, 314, 1121

63. Prasher, R. Thermal Interface Materials: Historical Perspective, Status, and Future Directions. Proc. IEEE 94, 1571–1586 (2006).

64. Wang, Yun, and Ken S. Chen. “Elucidating Two-Phase Transport in a Polymer Electrolyte Fuel Cell, Part 1: Characterizing Flow Regimes with a Dimensionless Group.” Chemical Engineering Science, vol. 66, no. 15, 2011, pp. 3557–3567., doi:10.1016/j.ces.2011.04.016.